

Granular flow through an aperture: Influence of obstacles near the outlet

M. G. Areán,¹ A. Boschan,² M. A. Cachile,² and M. A. Aguirre²

¹*Grupo de Medios Porosos, Fac. de Ingeniería, Universidad de Buenos Aires, Paseo Colón 850, (C1063ACV) Buenos Aires, Argentina*

²*Grupo de Medios Porosos, Fac. de Ingeniería, Universidad de Buenos Aires, CONICET, Paseo Colón 850, (C1063ACV) Buenos Aires, Argentina*



(Received 15 July 2019; accepted 20 December 2019; published 5 February 2020)

We study how the presence of obstacles in a confined system of monodisperse disks affects their discharge through an aperture. The disks are driven by a horizontal conveyor belt that moves at constant velocity. The mean packing fraction at the outlet decreases as the distance between the obstacles and the aperture decreases. The obstacles organize the dynamics of the stagnant zones in two characteristic behaviors that differ mainly in the magnitude of the fluctuations of the fraction of stagnant disks in the system. It is shown that the effective aperture is reduced by the presence of obstacles.

DOI: [10.1103/PhysRevE.101.022901](https://doi.org/10.1103/PhysRevE.101.022901)

I. INTRODUCTION AND BACKGROUND

Granular flows through an aperture have been intensely studied [1–12] due to their practical importance to several industries (e.g., pharmaceutical, mining, agriculture) and disciplines (e.g., chemistry, physics, engineering).

Depending on the ratio of outlet size to grain size, three regimes can be observed for the discharge of a silo through an orifice: a continuous flow, an intermittent flow, or a complete blockage of the system due to arching [13,14].

In the jamming regime, the jamming probability has been shown to be controlled by the ratio of aperture size to grain diameter [14–18] and it has been observed that the presence of an obstacle near the aperture reduces the jamming probability near the outlet and induces an increase in the flow rate [19–22]. Nevertheless, in the continuous regime, the influence of obstacles on the discharge rate has not been thoroughly studied, even if some works related to the discharge of silos have analyzed the influenced of inserts on the stress at the silos' walls and on inserts [23–29] and on flow pattern [24,25,27,30–33].

In particular, in the continuous-flow regime, generally observed for large outlets, the *mass flow rate* W is known to scale as $A^{5/2}$, where A is the diameter of the opening. This scaling, presented by Hagen in 1852 [34], is generally known as the Beverloo law [1,10,35]:

$$W = C\rho\sqrt{g}(A - kd)^{5/2}, \quad (1)$$

where ρ is the bulk density of the granular sample, g is the acceleration due to gravity, and d is the diameter of the grains. The parameters k and C are empirical dimensionless constants. It has been stated that the constant k accounts for boundary effects at the aperture edges, which leads to a boundary layer having a thickness of the order of the size of the grains (the so-called *empty annulus effect* [36]). Hence, an effective aperture, $A_{\text{eff}} \equiv A - kd$, is to be considered instead of A . Mankoc *et al.* introduced an exponential correction to Beverloo scaling to reconcile the empirical law with the experimental observations [13].

The Beverloo relation thus points out a value $A_c \equiv kd$ of the aperture size A at which the flow rate is expected to vanish. The value of k usually ranges from 1 to 3 depending on the grains and container properties [37]. Nevertheless, some works [13,38] claim that the only plausible value for k is 1. It should also be noted that Sheldon and Durian [39] stated that k is just a fitting parameter with no clear physical meaning, as they found clogging of the flow for apertures $A > kd$.

In a two-dimensional (2D) configuration one expects Beverloo's law to be $W = C\rho_{2D}\sqrt{g}(A - kd)^{3/2}$ [35].

In many industrial applications granular materials are transported horizontally, lying on conveyor belts [40] or floating on the surface of flowing liquids [41–43]. Recent works considered the discharge of a dense packing of disks driven through an aperture by a conveyor belt [44,45] driven at a constant velocity V . For large apertures ($A/d \geq 6$), the flow rate is continuous during the discharge.

A critical conveyor belt velocity V_c , independent of the size and mass of the disks, separates a low-velocity regime ($V < V_c$) where the flow rate is proportional to V and A and a high-velocity regime ($V > V_c$) where the flow rate is independent of V and proportional to $(A - kd)^{3/2}$ [45,46]. In this work, we present results obtained in the low-velocity regime where the mean exit velocity of the grains is $\langle V_g \rangle \cong V$. The number N of discharged disks depends linearly on time t , giving a constant flow rate $Q \equiv dN/dt$ (i.e., the number N of disks flowing out per unit time t), which obeys

$$Q = C\left(\frac{4}{\pi d^2}\right)V(A - kd), \quad (2)$$

where $k \simeq 2$ and the constant C reduces to the packing fraction [44]. Indeed, $\pi d^2/4$ is the surface area of one disk so that $C(4/\pi d^2)$ is the number of grains per unit surface which, multiplied by the belt velocity and by the size of the aperture, gives an estimate of the number of disks flowing out per unit time. Note that Eq. (2) is equivalent to the 2D Beverloo law in which the typical velocity $\sqrt{gA_{\text{eff}}}$, understood as the typical velocity of the grains at the outlet, is replaced by the belt velocity V because $\langle V_g \rangle \cong V$. It predicts that the

dimensionless flow rate $Q^* \equiv Qd/V$ is independent of V and increases linearly with the dimensionless aperture size A/d . It is interesting to note that this empirical law was demonstrated to be valid for small apertures $A/d < 6$, even if the system is likely to jam and deviations from linearity might be expected [44]. Indeed, in three-dimensional (3D) configurations, a marked deviation from the $5/2$ Beverloo scaling has been observed for very small apertures [13]. Moreover, previous works showed that, unlike fluid flows, granular flows are not governed by pressure at the outlet, but by the exit velocity of the grains [44,45]. The latter does not necessarily depend on the stress conditions in the outlet region, as proven by the experimental fact that, in gravity-driven systems, the typical velocity at the outlet is \sqrt{gA} , independent of the pressure. These observations were corroborated in vertical gravity-driven systems [47]. Also, it was observed [48] that, at least for a certain range of conveyor belt velocities V , the packing fraction C had no influence on grain velocity at the outlet, but it does modify the flow rate Q .

In the present article, we study the discharge process of monodisperse plexiglass rings (disks) driven through an aperture by a horizontal conveyor belt set at a constant velocity. In particular, we analyze if the presence of an obstacle or an array of obstacles has any type of influence on the packing fraction evolution or on the grain velocity near the outlet, and if they induce variations on the flow rate of grains driven by a horizontal conveyor belt through an aperture. Note that, in this horizontal system, as observed in previous works [44,45,48], it is easier to analyze the role that different factors have on the discharge process independently when the system is driven at a constant velocity (horizontal) or when it is gravity driven (vertical), such as, for example, corroborated by Perge *et al.* [47]. In fact, in the horizontal configuration, it is easier to control initial conditions and to measure grain velocity and packing fraction throughout the whole discharge process.

II. SETUP AND MEASUREMENT PROTOCOL

The granular material is composed of $N_o = 800$ plexiglass rings of thickness $e = (2.00 \pm 0.01)$ mm, internal diameter $d' = (2.00 \pm 0.01)$ mm, and external diameter $d = (4.00 \pm 0.01)$ mm. In particular, the inner holes of the rings are only used for detection purposes, during the image treatment, which will be explained below. The experimental setup (Fig. 1), similar to the one use in a previous work [48], consists of a conveyor belt made of black paper (width 110 mm $= 27.5d$, length 345 mm $= 86.25d$) above which a confining cardboard frame (inner width 90 mm $= 22.5d$, length 200 mm $= 50d$) is maintained at a fixed position in the frame of the laboratory. The cardboard frame provides smooth lateral walls. A motor drives the belt at a constant velocity V .

Downstream, the confining frame exhibits, at the center, a sharp aperture of width A . The aperture width can be tuned up to 90 mm but we shall report data obtained for a single width $A = (41 \pm 1)$ mm. The aperture size A is about 10 times greater than the grain diameter d , so that the condition insuring the continuous flow, $A/d \geq 6$, is satisfied [44].

The disks are imaged from top by means of a digital scanner (Canon, CanoScan LiDE 200) placed with its screen facing the frame, i.e., upside down. To focus on the top of

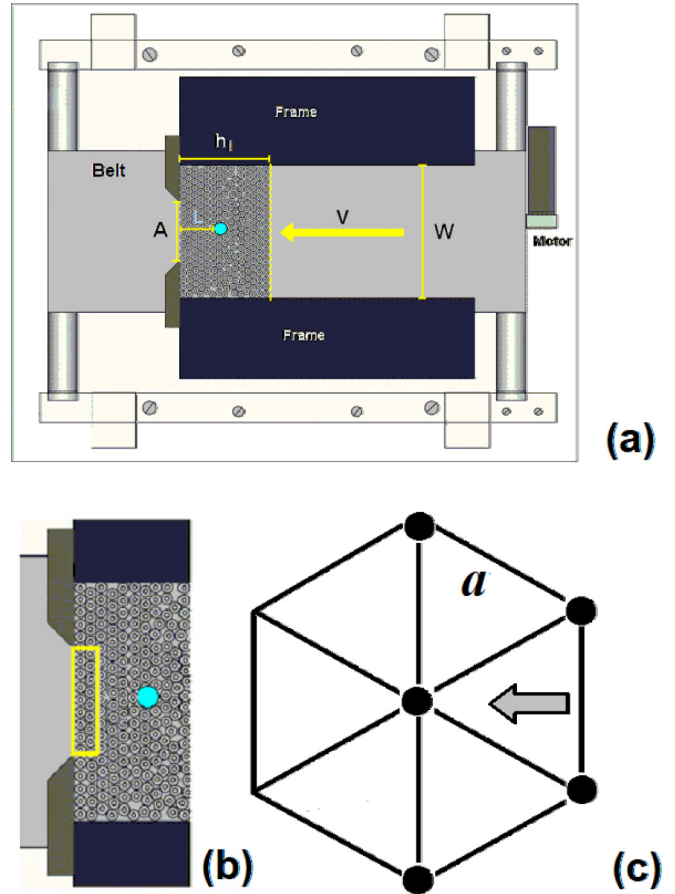


FIG. 1. (a) Sketch of the experimental setup. (b) Detail of the outlet zone. The rectangle indicated the region where the exit velocity and the packing fraction are measured. (c) Scheme of the array of obstacles: it consists of equilateral triangles with side of length $a = 41 \pm 0.1$ mm and five obstacles attached at vertices marked with dots. The arrow indicates the direction of the flow.

the disks without mechanical contact (space of about 1 mm between the scanner and the top of the disks) and thus avoid friction between the disks and the scanner window, the latter has been replaced by a thinner one, leading to a total gap between the screen and the conveyor belt of about $e_{\text{gap}} \simeq 3$ mm. The use of a scanner has the advantage of avoiding optical aberrations and makes it possible to obtain cheap, homogeneously lighted images with a high resolution (12 pixels/mm, the disk diameter being of the order of 50 pixels).

Plexiglass disks are used as obstacles and are glued on the scanner screen. In particular, obstacles have a thickness of $e_{\text{obstacle}} = (1.00 \pm 0.01)$ mm that ensures that, when the scanner is flipped over the conveyor belt, i.e., the frame, they do not make contact with it because the total distance from the screen to the conveyor belt is about $3e_{\text{obstacle}}$. Obstacles are fixed individually or ordered in an array, facing the center of the aperture and at a distance L from the outlet. The distance L can take six different values $L = iD$, with $i = 1, 2, 3, 4, 5$, or 6 and is measured from the outlet to the border of the obstacle facing the aperture with $D = 2d$. The granular packing might be prepared either with or without obstacles.

Experiments done without obstacles were used as a reference. In experiments with obstacles, they are placed in one of the following configurations:

i. One small plexiglass disk of diameter $D = (8.00 \pm 0.01)$ mm, i.e., $D = 2d$, and thickness $e = (1.00 \pm 0.01)$ mm at a distance L .

ii. One large plexiglass disk of diameter $D' = (12.00 \pm 0.01)$ mm, i.e., $D = 3d$, and thickness $e = (1.00 \pm 0.01)$ mm at a distance L .

iii. Array of five small plexiglass disks ordered, as shown in Fig. 1(c) in equilateral triangles with sides of length (4.10 ± 0.01) cm, which ensures that the distance between disks, i.e., obstacles, is greater than or equal to $6d$, enabling a continuous flow through them. The array is placed at a distance L being the row with 3 obstacles the nearest to the outlet.

Once one of the above configurations has been set, the system might be prepared in one of the following two initial conditions:

A. 800 grains (rings) are randomly closed packed upstream from the obstacle or array of obstacles (Fig. 2).

B. 800 grains (rings) are randomly closed packed from the outlet and surrounding the obstacle or obstacles in the array (Fig. 3).

In any of the cases mentioned above, the disks are placed over the conveyor belt and then the scanner, with the obstacles in the chosen configuration, is placed upside down over the belt. In particular, for studies with initial condition B, disks were placed all over the belt except where the obstacles were to be fit once the scanner was flipped in place. The latter is initially leaving a zone without disks around the obstacles (Fig. 3).

A typical initial response of the system to the conveyor belt motion can be seen on treated images in Figs. 2 and 3 (right panels) where the modulus of initial velocity vectors for each disk is presented for initial conditions presented for images on the left panels. At the beginning of the discharge process there is a transient (<5 s) where disks are arranging in wedge-like stagnant zones at each side of the aperture, as can be observed in right panels of Fig. 3. In Sec. III D, the fraction of stagnant grains will be studied for all systems, but it should be noted that the mentioned transient will be left out of the analysis.

Ten experiments were done for each configuration and each L value: 5 experiments with initial condition A and 5 experiments with initial condition B. In particular, for systems without obstacles 5 experiments were done with the only possible initial condition for this type of packings, i.e., initial condition B.

After preparing the system, the discharge is then initiated by setting the belt velocity V to a fixed chosen value. It fact, small fluctuations in setting the voltage controlling the conveyor belt velocity led to experiments where $V = (11.5 \pm 0.5)$ mm/s ($V = 2.75$ d/s).

During the discharge process in the continuous steady regime, i.e., as long as grains fill a distance of $2D$ upstream of the outlet, the disks rearrange as the conveyor belt slides beneath them until they reach the outlet where they lose contact with neighbors and are set free from the packing. As mentioned in Sec. I, a critical conveyor belt velocity V_c separates a low-velocity regime ($V < V_c$) where the flow rate is proportional to V and A from a high-velocity regime

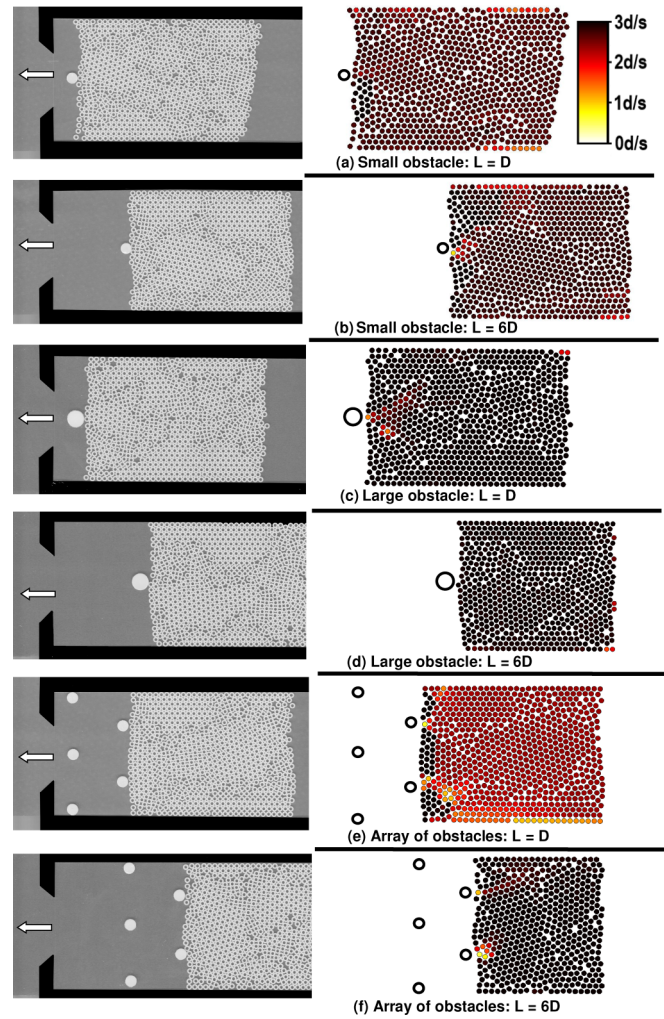


FIG. 2. Panels in the left side show snapshots of granular packing with initial condition A. Panels (a) and (b) System with a small obstacle placed at $L = D$ and $L = 6D$, respectively. Panels (c) and (d) System with a large obstacle placed at $L = D$ and $L = 6D$, respectively. Panels (e) and (f) System with an array of small obstacles placed at $L = D$ and $L = 6D$, respectively. White arrows indicate the direction of the conveyor belt motion. Panels at the right side show treated images indicating the modulus of the initial velocity vector for each disk: the small circles pinpoint the position of each disks and its color indicates their modulus of velocity. For all images at the right, the reference of colors is given in the right panel (f); velocities are in d/s. Note that belt velocity $V \approx 2.75$ d/s. In all panels, the position of obstacles is indicated with a black ring.

($V > V_c$) where the flow rate is independent of V and proportional to $(A - kd)^{3/2}$ [45,46]. These different regimes appear from the competition between two characteristic timescales: the time needed for a disk to stop on the belt after losing contact with packing and the time it takes to reach the aperture. According to Cordero and Pugnaroni [46], $V_c = 0.92\sqrt{g\mu A}$. So, considering a dynamic friction coefficient $\mu = 0.5$, the estimated critical velocity for this experimental system ($A \approx 10d$) is $V_c \approx 407$ mm/s ($V \approx 102$ d/s). Therefore, being in the low-velocity regime ($V < V_c$) we expect that the mean exit velocity of the grains, $\langle V_g \rangle \cong V$, and that the flow rate Q will

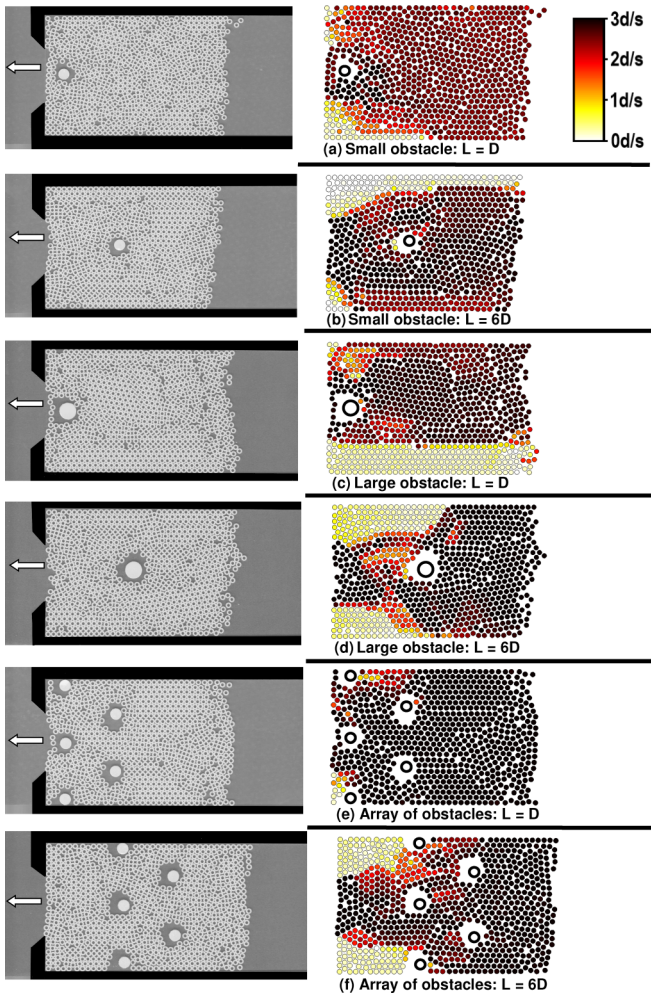


FIG. 3. Panels at the left side show snapshot of granular packing with initial condition B. Panels (a) and (b) System with a small obstacle placed at $L = D$ and $L = 6D$, respectively. Panels (c) and (d) System with a large obstacle placed at $L = D$ and $L = 6D$, respectively. Panels (e) and (f) System with an array of small obstacles placed at $L = D$ and $L = 6D$, respectively. White arrows indicate the direction of the conveyor belt motion. Panels at the right side show treated images indicating the modulus of the initial velocity vector for each disk: the small circles pinpoint the position of each disks and its color indicates their modulus of velocity. For all images at the right, the reference of colors is given in the right panel (f); velocities are in d/s . Note that belt velocity $V \approx 2.75 d/s$. In all panels, the position of obstacles is indicated with a black ring.

be proportional to the belt velocity, as described by Eq. (2). The latter will be analyzed in Secs. III A and III B.

The evolution of the discharge process is assessed by repetitively moving the belt at the chosen constant velocity V during a time interval $dt = 0.1$ s and by recording an image from the scanner while the belt is at rest. The conveyor belt color presents inhomogeneities (texture) that allows us to apply particle image velocimetry in order to measure its velocity during the discharge process. For each experiment the belt velocity V is characterized by the mean velocity $\langle V \rangle$ evaluated with the first 50 consecutive images of the discharge process.

For the present study, image analysis is used to determine the position of each grain inside the system during the discharge process. Those measurements allow us to determine the flow rate (Q) during the discharge process, the packing fraction (C) evolution near the outlet, and the grain velocity inside the confining frame and, in particular, near the outlet [exit velocity of grains, V_g ; see Fig. 1(b)]. In each frame registered during a discharge process is analyzed by using the software ImageJ [49], an intensity threshold is used to convert each image into binary: white is assigned to the rings (grains) and black is assigned to the background. Therefore, black disks at the center of each grains are isolated from one another, which makes it easy to detect them and to compute, for each frame (time t),

i. the number of grains remaining in the frame, N_{in} , or, equivalently, the number of disks that flowed out the system at time t , $N \equiv N_o - N_{in}$. The instantaneous flow-rate (averaged over $dt = 0.1$ s, because of the acquisition rate) is defined as $Q = dN/dt$.

ii. the position of grains remaining inside the confining frame, which allows us to determine its trajectories and velocities as well as the packing fraction by using Voronoi tessellation.

In particular, packing fraction evolution is analyzed near the outlet. In a region of width A and thickness $2d$ upstream of the aperture [Fig. 1(b)], a Voronoi tessellation is made, for each frame of the discharge process: each grain j (with surface $S_g = \frac{\pi d^2}{4}$) allows us to define a packing fraction value $C_j = S_g/S_V$ in its Voronoi cell of surface S_V . Therefore, the packing fraction in the region of interest can be characterized with the mean value $\langle C \rangle$ of the different values C_j .

Concerning the measurement of the exit velocity of the grains through the aperture, a mean value V_g , calculated with velocities of disks inside a region near the outlet, is obtained for each frame (time) registered during all the discharge processes.

Another topic of interest is the ratio or fraction of stagnant grains F_s inside the confining frame at any given time (frame), which requires measuring the number of stagnant disks in relation to the total number of disks at a given frame (time). The latter is obtained by analyzing how many disks have not moved from one frame (i) to the following one ($i + 1$), i.e., between two successive frames. Therefore, with ImageJ [49], intensity of consecutive frames is averaged giving a resulting image where disks that have moved are blurred and have a high eccentricity ε while stagnant disks have sharp edges and $\varepsilon < 0.1$ which allows us to clearly detect how many stagnant disks (N_s) were in frame i . Note that this method can detect motion of disks that have moved 3 pixels (less than 7% of its diameter) between frames ($\Delta t = 0.1$ s), i.e., disks moving with $V_g > 0.065 d/s$ are not considered as stagnant particles.

The fraction of stagnant grains at a given time (frame i) is $F_s(i) = N_s/N_i$, where N_i is the total number of grains (disks) in frame i .

III. EXPERIMENTAL RESULTS

The discharge process is analyzed during the continuous steady regime, i.e., as long as grains fill a distance of $2D$ upstream of the outlet. Also, experiments with initial

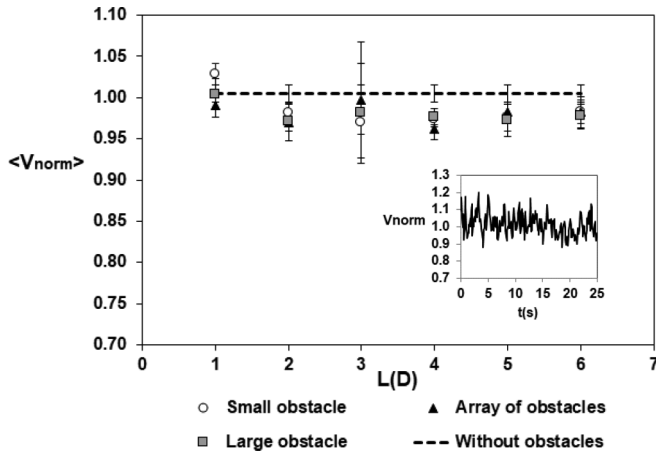


FIG. 4. Mean normalized velocity of the disks at the outlet, $\langle V_{\text{norm}} \rangle$, for all configurations, i.e., without obstacles and with obstacles (small single obstacle, large single obstacles, and array of small obstacles) placed at different distances L from the outlet. Error bars correspond to the standard deviation of the set of data corresponding to each configuration. Inset shows an example of the evolution of V_{norm} during the discharge process while in the steady regime; the data correspond to a system with one small obstacle placed at $L = D$.

condition A have a transient until the disks arrive at the outlet (i.e., start flowing out of the system), and this transient regime is discarded in the analysis.

A. Exit velocity

The exit velocity of disks through the aperture is measured as explained in Sec. II, i.e., during the discharge process. For each frame, a mean value V_g is obtained from velocities of disks near the outlet [Fig. 1(b)]. To be independent of variations in the tuning of the voltage controlling the velocity of the conveyor belt in different experiments, V_g is normalized by $\langle V \rangle$, which, as explained in Sec. II, is the mean velocity of the belt evaluated over the first 50 consecutive images of the discharge process.

For each configuration, as mentioned in Sec. II, several experiments were made and the evolution of $V_{\text{norm}} = V_g / \langle V \rangle$ was obtained. A typical evolution of V_{norm} is shown in the insert of Fig. 4; in all cases, velocities are registered while there is a steady flow rate, i.e., while grains fill a distance of $2D$ upstream of the outlet.

It can be noted that V_{norm} oscillates around 1. For each configuration, a mean value $\langle V_{\text{norm}} \rangle$ was obtained considering all the experiments, regardless of their initial condition, and results are presented in Fig. 4. Absolute errors are estimated from the standard deviation of the set of data corresponding to each configuration and they give relative percent errors less than 2% for almost every case except for systems with an array or a big obstacle placed at $L = 3D$ where the relative percent errors are less than 7.1%. Therefore, it can be stated that, for all configurations, $\langle V_{\text{norm}} \rangle \approx 1$ within the error bars, indicating that grains are discharged through the outlet with a mean velocity $\langle V \rangle$, i.e., the velocity imposed by the conveyor belt. The latter was already observed in previous works [46,48] and is expected if the velocity V is low.

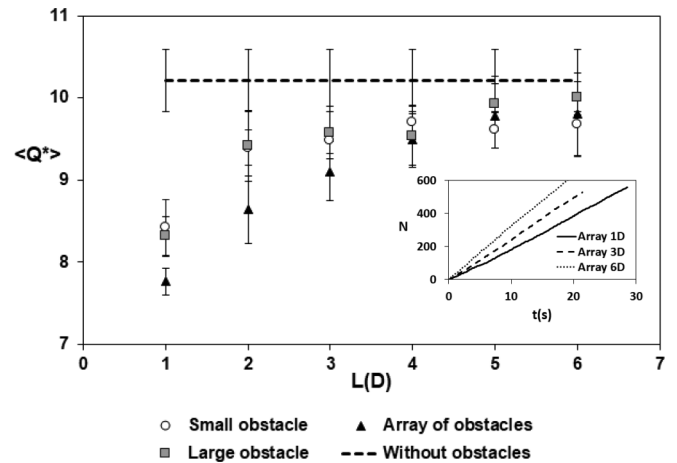


FIG. 5. Dimensionless mean flow rate $\langle Q^* \rangle = \langle Q \rangle d / \langle V \rangle$ for all configurations, i.e., without obstacles and with obstacles (small single obstacle, large single obstacles, and array of small obstacles) placed at different distances L from the outlet. Error bars correspond to the standard deviation of the set of data corresponding to each configuration and correspond to a relative percent error of approximately 3%. Dashed line corresponds to $\langle Q^* \rangle$ obtained in a packing without obstacles and it is placed for the purpose of comparison.

B. Flow rate

Concerning the flow rate, it is observed that the number N of grains that flows out of the system as a function of time t is linear (see inset to Fig. 5), i.e., a constant flow rate Q . It has been found that Q is not influenced by the initial condition. Therefore, for each configuration a mean value $\langle Q \rangle$ was obtained by considering all the experiments, regardless of their initial condition.

Also, as already mentioned in the previous section and also observed in previous works [46,48], while the conveyor belt is driven at a low velocity V , it controls the exit velocity of the grains during the discharge process. As already mentioned, variations in the tuning of the voltage of the motor would lead to fluctuations in the mean velocity $\langle V \rangle$ that characterizes the belt velocity and therefore the mean value of the velocity at which the grains are discharged (V_g). Therefore, to be independent of the belt velocity, a dimensionless mean flow rate $\langle Q^* \rangle = \langle Q \rangle d / \langle V \rangle$ is measured and the results are presented in Fig. 5 for all the configurations. It can be observed that the flow rate increases with distance L and reaches an asymptotic value for obstacles placed at $L \geq 5$. Note that, for all configurations, the flow rate is always lower than without obstacles, indicating that the obstacles still exert influence for all the configurations studied in this work. Also, the size of the obstacles that were used does not affect the flow rate, but increasing the number of obstacles (configuration with obstacles in an array) slightly diminishes the flow rate when the obstacles are placed near the outlet.

C. Packing fraction

It has been observed in a previous work that the flow rate is influenced by the packing fraction C near the outlet [48]. Therefore, we measure the packing fraction upstream of the aperture [Sec. II and Fig. 1(b)] during the steady regime of the

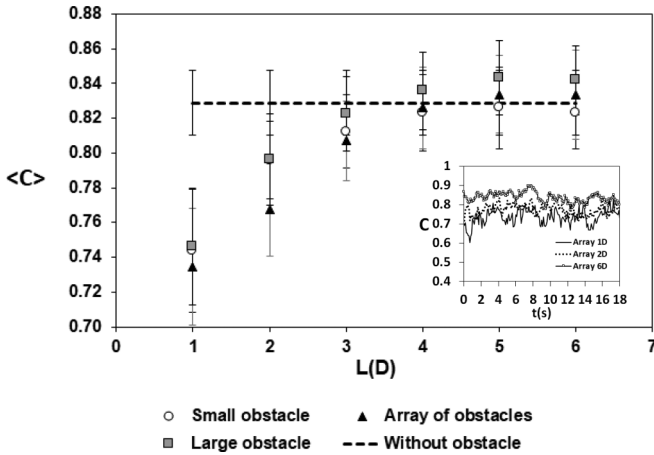


FIG. 6. Mean packing fraction $\langle C \rangle$ in the outlet region for all configurations, i.e., without obstacles and with obstacles (small single obstacle, large single obstacles, and array of small obstacles) placed at different distances L from the outlet. Error bars correspond to the standard deviation of the set of data corresponding to each configuration. The dashed line corresponds to $\langle C \rangle$ obtained in a packing without obstacles and is placed for the purpose of comparison.

discharge process. It has been found that C is not influenced by the initial condition and that, during the discharge process, it presents small oscillations around a constant value that depends on the configuration of obstacles. Therefore, for each configuration, a mean value $\langle C \rangle$ was obtained considering all the experiments regardless of their initial condition, and the results are presented in Fig. 6. Absolute errors are estimated with the standard deviation of the set of data corresponding to each configuration and they give relative percent errors less than 5% for any case, being the largest (4.5 ± 0.2)% for configurations of obstacles placed at $L = D$. It can be observed that $\langle C \rangle$ increases with the obstacle's distance L to the exit and reaches an asymptotic value for obstacles placed at $L \geq 4$. Since the flow rate is proportional to C [Eq. (2)] and considering the results in Sec. III B and Fig. 5, it was expected that the packing fraction for systems without obstacles would also be higher than in packings with obstacles for $L \geq 5$, but a different behavior is observed in Fig. 6: the discharge of granular packings in the presence of obstacles might reach a higher packing fraction at the outlet than the system without obstacles, indicating that the effective aperture size $A_{\text{eff}} \equiv A - kd$ and therefore k are affected by the presence of obstacles. It should be noted that, with or without obstacles, the mean packing fraction asymptotic value C_{asim} is slightly larger than the packing fraction corresponding to random dense packings, i.e., 0.82 [50], indicating the presence of ordered clusters (hexagonal ordered disks have a packing fraction of approximately 0.91 [50]).

D. Fraction of stagnant grains

During the discharge of packings without obstacles, disks are retained at each side of the outlet, forming wedge-like stagnant regions that enhance the presence of stalled disks that stack in ordered arrays along the lateral walls; we will refer to both zones (wedge-like and lateral ordered regions)

as *extended lateral stagnant zones*. Particles in the wedge-like zones are not permanently stalled since they are slowly displaced by those moving upstream of the wedges. Eventually, when only disks in the stagnant zone are remaining inside the system, they are also slowly driven out through the outlet by the motion of the conveyor belt but, the system being in the nonsteady regime, i.e., nonconstant flow rate, data from this last part of the discharge process is not considered. Note that, at the beginning of the discharge, there is a transient (< 5 s) where disks are arranging in the wedge-like stagnant zones, and this transient will also be left out of the analysis.

It is expected that the presence of obstacles will modify the number of particles that get stalled in the system during the discharge process. Effectively, in systems with obstacles, apart from the wedge-like stagnant zones at each side of the outlet and the ordered disks stalled along the lateral walls (examples can be observed in the right panels of Fig. 3), disks are also stuck behind the obstacles, although not permanently because eventually they are replaced by ones moving upstream from each obstacle (an example can be observed in right panels of Fig. 13).

The ratio or fraction of stagnant grains F_s inside the confining frame is analyzed during the discharge process for all configurations. As mentioned in Sec. II, F_s is defined as $F_s(i) = N_s/N_i$, with N_s being the number of stagnant disks and N_i being the total number of disks remaining in the packing at a given time (frame i). F_s presents two different types of behavior in the steady regime, i.e., while the flow rate is constant:

Type I. F_s presents large fluctuations, which nevertheless allow us to define a mean value F_s^{mean} after the transient where the wedge-like stagnant zones are formed and while in the steady-flow-rate regime. F_s^{mean} is used to characterize these discharge processes. An example is shown in the top panel of Fig. 7.

Type II. F_s presents a linear increase with small fluctuations around a linear trend, that might be fit with a slope S_s and an intercept I_s , which are used to characterize these discharge processes. An example is shown in the bottom panel of Fig. 7. In some cases, before the linear behavior appears a transient with large fluctuations, similar to type I, might be observed.

On the one hand, experiments showing type-I behavior present 50% of their fluctuations that are larger than 15% of F_s^{mean} . On the other hand, experiments showing type-II behavior present 50% of their fluctuations with respect to the fitted line that are 10% smaller than the fitted values. The clear difference in the size of fluctuations allows us to distinguish and classify experiments presenting type-I behavior from those with type-II behavior.

Large fluctuations of F_s can be related to important variations in the size of the lateral ordered zones that are strongly affected by the presence of obstacles. On the one hand, if obstacles are placed near the outlet they affect these lateral zones by producing fluctuations in the wedge-like zones that propagate upstream to these lateral zones. On the other hand, if obstacles are further away from the outlet, they induce lateral flows that perturb these lateral stagnant zones.

Recall that N_i decreases linearly during the discharge process while it is in the steady regime and, therefore, type-I

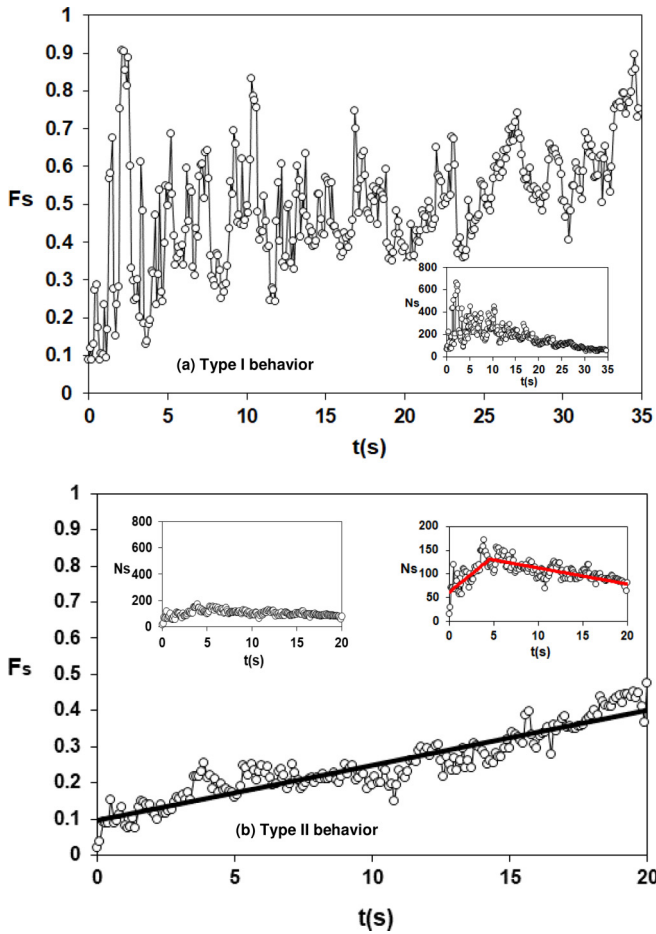


FIG. 7. Examples of the evolution of the stagnant fraction F_s are presented for type-I and type-II behaviors. The top panel (a) corresponds to the discharge in the presence of a small obstacle placed at $L = D$. Inset: shows a variation of the number N_s of stagnant particles during the discharge process. The bottom panel (b) corresponds to the discharge in the presence of an array of obstacles placed at $L = 5D$. Left inset shows the variation of the number N_s of stagnant particles during the discharge process. Right inset shows a zoom of the inset at the left with tendency line.

behavior can be associated with a decrease in the number of stagnant disks [see inset of panel (a) of Fig. 7] caused by the presence of obstacles that, despite the large fluctuations, are on average reducing the size of the stagnant zones, especially the so-called *extended lateral stagnant zones*.

On the other hand, type-II behavior during the discharge process is due to the presence of stagnant zones covering a total mean area, which during a short transient increases or remains approximately constant and then decreases [see inset of panel (b) of Fig. 7]. To observe the linear increase in F_s , during the discharge the number N_s of stagnant disks should be decreasing slower than the disks remaining in the system (N_i), i.e., N_s can be assumed to be approximately constant. The short transient, which is absent in some experiments, is due to perturbations induced by obstacles in the *extended lateral stagnant zones*, i.e., presents a type-I behavior.

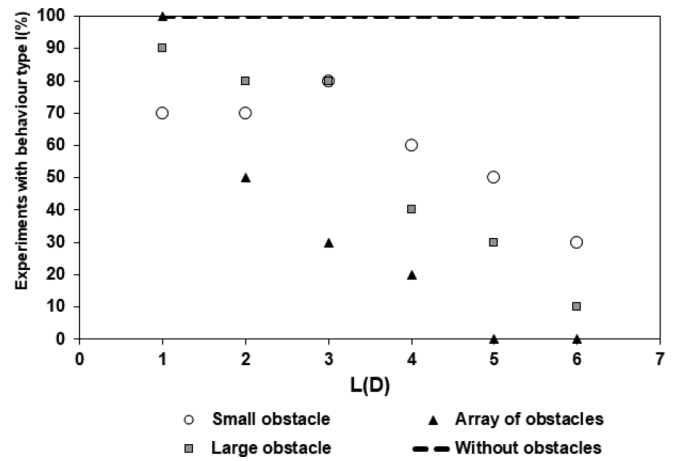


FIG. 8. Percentage of experiments, for each configuration, showing type-I behavior. Dashed line corresponds to the percentage of experiments obtained in a packing without obstacles and it is placed for the purpose of comparison.

Figure 8 shows the percentage of experiments, for each configuration, showing type-I behavior. It should be noted that the percentage of experiments with type-II behavior is the complement of the data shown in Fig. 8. Concerning experiments without obstacles, all of them presented a type-I behavior indicating that the *extended lateral stagnant zones* are being eroded during the discharge process.

For experiments with obstacles, in all configurations, the proportion of type-I behavior experiments decreases as the obstacles are displaced at large distances from the outlet. Effectively, the presence of obstacles enhances the erosion of the *extended lateral stagnant zones* and in particular the stagnant wedges because, during the discharge process, they are redirecting the flow to these stagnant zones.

In fact, on the one hand, for an array of obstacles at $L = 1D$, all the experiments presented a decrease of the *extended lateral stagnant zones* during the discharge, i.e., type-I behavior, and this behavior completely disappears when the array is placed at $L \geq 5D$.

On the other hand, in systems with a single obstacle, there is a larger probability that systems with the smaller obstacle at $L < 3D$ get the stagnant wedges eroded due to a larger gap between the obstacle and the stagnant zone that enhances erosion because it facilitates the displacement of disk into these regions. Nevertheless, as shown below (Fig. 9), once the flow has been redirected near the stagnant zones, a larger erosion (fewer stalled disks) takes place in the presence of a larger obstacle. As mentioned, perturbations of the stagnant wedges will affect all *extended lateral stagnant zones*.

On the contrary, smaller obstacles placed at $L > 3D$ are less effective in producing a decrease of the stagnant zones and therefore type-I behavior is less probable (<50%). It can also be observed that the largest obstacle needs to be placed farther away from the outlet in order to lose effectiveness in decreasing the stagnant zones (type-I behavior), in fact, type-I behavior is less probable than type-II when the obstacle is as far as $L > 5D$.

Finally, an interesting fact to be noticed in Fig. 8 is that, as L increases, F_s does not behave like in the absence of

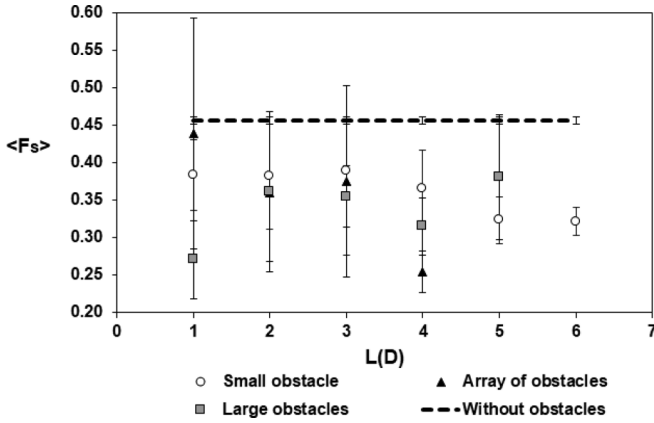


FIG. 9. Average $\langle F_s \rangle$ for each type of configuration presenting type-I behavior. Dashed line corresponds to the average value $\langle F_s \rangle$ obtained in experiments in a packing without obstacles and it is placed for the purpose of comparison.

obstacles, showing that the presence of obstacles still affects the flow even if they are situated far from the aperture. This counterintuitive result may be due to the influence of flow confinement.

1. Type-I behavior

Each experiment showing type-I behavior can be characterized by F_s^{mean} , and mean values $\langle F_s \rangle$ taken for each type of configuration are presented in Fig. 9. Note that systems with an array of obstacles placed at $L = D$ present a fraction F_s that behaves as in packing without obstacles: all the experiments present a type-I behavior and the average value $\langle F_s \rangle$ is similar. The latter might be explained by considering that obstacles near the wedge-like stagnant zones (see Fig. 2) are right next to the wall and are not affecting the erosion of the wedges, and obstacles in the second row seem to compensate the erosion produced by the central obstacle in the first row facing the aperture. Otherwise, experiments without obstacles show, on average, a proportion of stagnant disks ($24 \pm 9\%$) larger than in systems with obstacles with type-I behavior, indicating that obstacles are modifying boundary conditions that are mostly enhancing the erosion of the wedge-like stagnant zones. Even if placed far from the outlet, they are decreasing $\langle F_s \rangle$ by diminishing the ordered stagnant regions besides the lateral walls and therefore, the whole *extended lateral stagnant zones*. As already mentioned, it should be noted that the discharge of packing with a single large obstacle presents the smallest $\langle F_s \rangle$ (largest erosion).

2. Type-II behavior

Systems where the fraction F_s of stagnant disks present, at some point of the discharge process, a linear increase (type-II behavior) can be characterized with the slope S_s and the intercept I_s obtained by a least squares regression method. The intercept I_s indicates a mean value of the stagnant fraction when the linear regime begins. As can be observed in Fig. 10, its value is equally affected by the presence and position of obstacles, so all configurations can be characterized with a mean value $\langle I_s \rangle = 0.19 \pm 0.04$. Values of the slope S_s , for

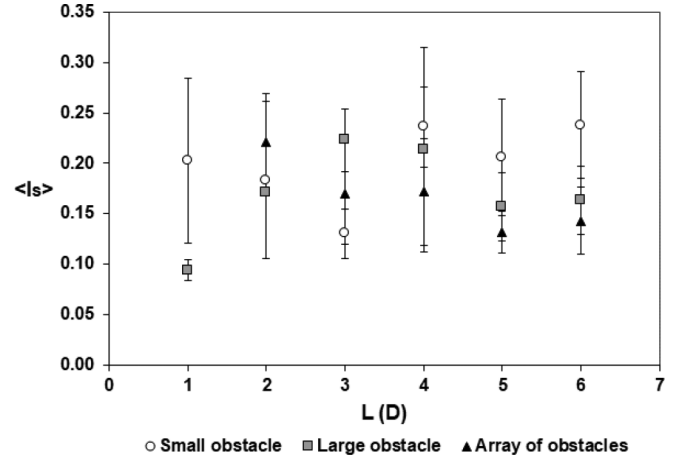


FIG. 10. Average value of the intercept $\langle I_s \rangle$ obtained from the linear least square fit of F_s as a function of time, for each type of configuration presenting type-II behavior.

all configuration are presented in Fig. 11. The value of the slope S_s is approximately the same for every configuration with obstacles placed at a given L value. In particular S_s increases with L up to $L \leq 3D$ then an asymptotic value, $\langle S_s \rangle = (0.016 \pm 0.002) \text{ s}^{-1}$, is reached.

IV. DISCUSSION AND CONCLUSIONS

In this work, we have analyzed the discharge process of a two-dimensional packing of monodisperse disks in the presence of different configurations: a single obstacle (big and small) or an array of obstacles placed in front of the outlet at different distances.

The flow rate described by Eq. (2) indicates that flow rate is not only proportional to packing fraction but also to $(A - kd)$, where k , as discussed in Sec. I, can be interpreted as a fitting parameter that leads to an effective aperture $A_{\text{eff}} = A - kd$ influenced by boundary effects. Results obtained in Sec. III indicate that the boundary condition at the outlet is influenced by the presence of obstacles. Moreover, the fact

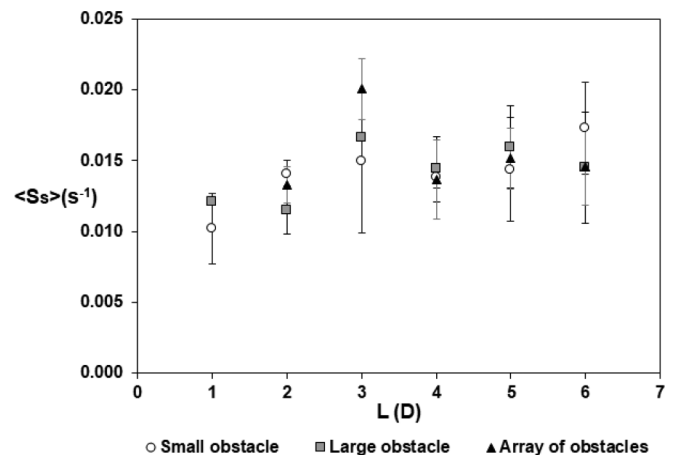


FIG. 11. Average value of the slope $\langle S_s \rangle$, obtained from the linear least square fit of F_s as a function of time, for each type of configuration presenting type-II behavior.

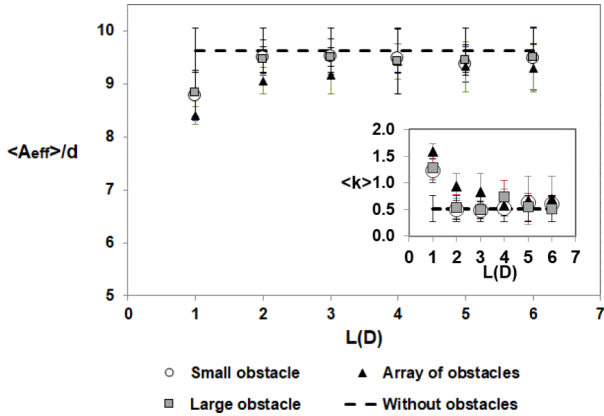


FIG. 12. Average effective aperture $\langle A_{\text{eff}} \rangle$ for all configurations, i.e., without obstacles and with obstacles (small single obstacle, large single obstacles, and array of small obstacles) placed at different distances L from the outlet. Dashed line corresponds to $\langle A_{\text{eff}} \rangle$ obtained in a packing without obstacles and it is placed for the purpose of comparison. Inset shows the average $\langle k \rangle$ for all configurations.

that, for systems with obstacles, the asymptotic value $\langle Q^* \rangle$ is below the one obtained in systems without obstacles while the asymptotic value for $\langle C \rangle$ is above, indicates that A_{eff} varies for different configurations and, therefore, mean values for the effective aperture $\langle A_{\text{eff}} \rangle = \pi d^2 \langle Q \rangle / (4V \langle C \rangle)$ were obtained for all configurations. This effective aperture can be expressed in terms of the particle diameter d , and Fig. 12 definitely shows that the presence of obstacles affect boundary conditions and $\langle A_{\text{eff}} / d \rangle$ is smaller than in systems without obstacles where $\langle A_{\text{eff}} / d \rangle = 9.6 \pm 0.4$, slightly smaller than the real aperture $A/d = 10.3 \pm 0.3$. It is also observed that an array of obstacles has a stronger influence up to $L = 4D$ where a constant value, slightly smaller than in other systems, is reached. For configurations with a single obstacle a constant $\langle A_{\text{eff}} / d \rangle$ value is reached for $L \geq 2D$. The inset in Fig. 12 shows that $\langle k \rangle = (\langle A_{\text{eff}} \rangle - A) / d$ reaches an asymptotic maximum value for the array of obstacles and for single obstacles that are, respectively, 50%, 250%, and 300% larger than the value of the system without obstacles where $\langle k \rangle = 0.5 \pm 0.2$. Note that, if k is not taken just as a fitting parameter [39], an increase of 300% of k , even if it seems large, indicates that the aperture is reduced in approximately 1.5 disk diameters d with respect to the situation without obstacles and decreasing the flow rate in approximately 2 disks per second, which is the observed variation in $\langle Q \rangle$ (Sec. III B). This decrease in real aperture, for obstacles near the outlet, can be explained by the low-packing-fraction regions that appear downstream (in front) of the obstacles and that are affecting boundary conditions at the outlet.

The flow rate is found to be always smaller than that in the absence of obstacles and is strongly influenced when obstacles are placed very near the outlet at $L = D$. As can be seen in Fig. 13, disks flow bordering the obstacle facing the outlet, i.e., centered obstacle, and are discharged as if by two smaller apertures [indicated with two dashed segments over the left panel of Fig. 13(a)]. The size of these two smaller slots is $l \approx 5d$ for small or large obstacles. Note that disks coming from different sides of the obstacle do not interact

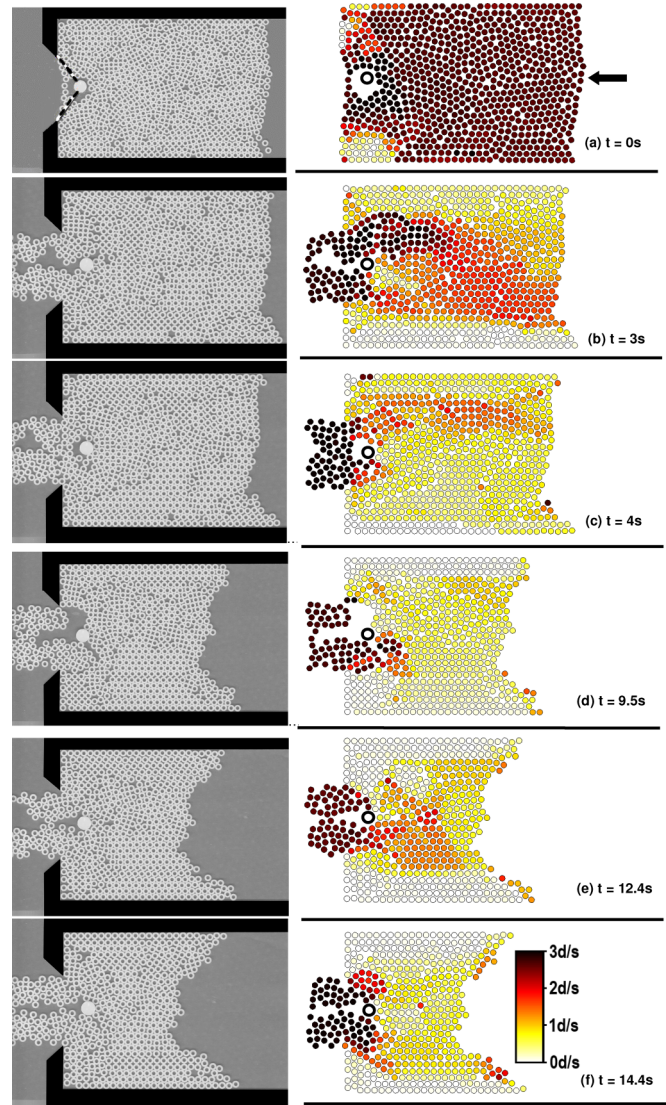


FIG. 13. Panels at the left side show snapshots taken during the discharge process in a system with a small obstacle placed at $L = D$. The obstacle splits the outlet into two smaller slots whose position is highlighted with dashed lines in the image in the panel (a) at the left side. Panel (b) The jet of discharged disks is split. Panels (c) and (e) There is small probability for split jets to merge. Panel (d) Transient arches that form at the smaller slots produce a splitting of the discharge jet. Black arrow on the right of panel (a) indicate the direction of the conveyor belt motion. Panels on the right side show treated images indicating the modulus of the velocity vector for each disk: the small circles pinpoint the position of each disk and the color indicates the modulus of the velocity. For all images at right, the color bar is given in the right side of panel (f); velocities are in d/s . Note that belt velocity $V \approx 2.75 d/s$. In all panels, the position of obstacles is indicated with a black ring.

and produce a low-packing-fraction zone (Fig. 6). In fact, in the limit of $L = 0$, a single small (large) obstacle will split the outlet into two smaller apertures of size $l/d = 4$ ($l/d = 2.5$). Although this experimental configuration was not explored, it is expected to lead to a strong decrease of the flow rate with respect to a system without obstacles and to increase the probability of blockage or jamming at the outlet. In particular, the mentioned splitting of the outlet in two smaller slots,

should be considered in understanding the decrease of A_{eff} and (C) observed for small L values (Fig. 12).

The following observations have been made in configurations placed at $L = D$:

i. With a small obstacle: Several times during the discharge process, the jet of disks flowing through the outlet splits into two smaller ones which later merge. Splitting and merging can be explained by two competing factors. On the one hand, there is a tendency of the system to transitory jam at the smaller slots, which will lead to splitting [Fig. 13(d)]. On the other hand, disks from each side of the obstacle tend to accumulate in front of the obstacle, filling the empty area between the two lateral jets, which leads to their merging.

ii. With a big obstacle: The empty area in front of the obstacle separating the lateral jets is larger, so it is rare to observe merging of the flow coming from smaller slots because there is not enough accumulation of disks in that zone.

iii. With an array of obstacles: Merging of the flow coming from smaller slots has not been observed. The latter might be understood considering that the two obstacles that are upstream from the centered one induce, downstream, low-packing-fraction zones that lead to a smaller flow rate through the lateral slots and, therefore, there is not enough accumulation of disks to produce the merging of the flow.

In general, after a transient of a few seconds, the splitting disappears in systems with a single obstacle at $L \geq 2D$ and with an array of particles at $L \geq 3D$. In particular, a detailed analysis of the mentioned transient is beyond the scope of this work, but we observed that, during the transient, the jets of disks coming from the side of the obstacle facing the outlet successively merge and split until a stable single front of disks exits the system through the aperture of the box.

Finally, variations of the stagnant fraction during the discharge process are mainly due to modifications of the wedge stagnant zones affected by the presence of obstacles but are not directly influenced by the particles stalled behind the obstacles.

In summary, the flow rate and the packing fraction in the outlet region of a discharging $2D$ silo have been simultaneously measured in the presence of a single obstacle or an array of obstacles. It has been found that obstacles mainly affect the boundary condition at the outlet even if placed at the largest distance studied, $L = 6D$. Therefore, obstacles induce a decrease of the effective aperture, the flow rate, and the packing fraction at the outlet for $L \leq 4D$ while an increase in packing fraction is observed for larger L values. The latter might be explained by considering that systems with obstacles present smaller stagnant fraction values which are mainly due to the reduction of the wedge-stagnant zones and, therefore, more mobile disks are arriving at an effective smaller outlet which induces an increase of the packing fractions at the outlet for $L > 4D$.

In many practical situations, silos are used to store grain, and it has been proposed to use inserts to modify the type of flow (from mass to funnel) and avoid blockages. In particular, there are several works that analyze the influence of inserts on the stress at the silos wall and on inserts [23–29] and on flow pattern [24,25,27,30–33], but there are insufficient studies of how the placement of an insert too near or too far from the outlet might affect the discharge rate [31,51,52]. This work is expected to provide knowledge of the flow rate of disks in the presence of obstacles while in the continuum and steady discharge regime and on how stagnant zones affect boundary conditions at the outlet.

ACKNOWLEDGMENTS

We acknowledge fruitful discussions with Dr. Irene Ippolito, Dr. Marcelo Piva, and Dr. Germán Drazer. This work was supported by the program UBACyT 20020130100490BA (University of Buenos Aires) and CAFCI (Argentine-France International Cooperation Program CONICET-CNRS). M.A.A. acknowledges support from CONICET and M.G.A. acknowledges support from the Program “Inserción Laboral Universitaria” (PILU - FIUBA).

-
- [1] W. A. Beverloo, H. A. Leninger, and J. van de Valde, *Chem. Eng. Sci.* **15**, 260 (1961).
- [2] L. P. Kadanoff, *Rev. Mod. Phys.* **71**, 435 (1999).
- [3] P. G. de Gennes, *Rev. Mod. Phys.* **71**, S374 (1999).
- [4] V. Trappe, V. Prasad, L. Cipelletti, P. N. Serge, and D. A. Weitz, *Nature (London)* **411**, 772 (2001).
- [5] H. M. Jaeger, S. R. Nagel, and R. P. Behringer, *Rev. Mod. Phys.* **68**, 1259 (1996).
- [6] J. Duran, *Sands, Powders and Grains* (Springer, New York, 2000).
- [7] G. H. Ristow, *Pattern Formation in Granular Materials* (Springer, New York, 2000).
- [8] R. M. Nedderman, U. Tüzün, S. B. Savage, and G. T. Houlsby, *Chem. Eng. Sci.* **37**, 1597 (1982).
- [9] U. Tüzün, G. T. Houlsby, R. M. Nedderman, and S. B. Savage, *Chem. Eng. Sci.* **37**, 1691 (1982).
- [10] R. M. Nedderman, *Statics and Kinematics of Granular Materials* (Cambridge University Press, 1992).
- [11] S. B. Savage, R. M. Nedderman, U. Tüzün, and G. T. Houlsby, *Chem. Eng. Sci.* **38**, 189 (1983).
- [12] B. P. Tighe and M. Sperl, *Granular Matter* **9**, 141 (2007).
- [13] C. Mankoc, A. Janda, R. Arévalo, J. M. Pastor, I. Zuriguel, A. Garcimartín, and D. Maza, *Granular Matter* **9**, 407 (2007).
- [14] C. Mankoc, A. Garcimartín, I. Zuriguel, D. Maza, and L. A. Pugnaloni, *Phys. Rev. E* **80**, 011309 (2009).
- [15] K. To, P.-Y. Lai, and H. K. Pak, *Phys. Rev. Lett.* **86**, 71 (2001).
- [16] I. Zuriguel, L. A. Pugnaloni, A. Garcimartín, and D. Maza, *Phys. Rev. E* **68**, 030301(R) (2003).
- [17] I. Zuriguel, A. Garcimartín, D. Maza, L. A. Pugnaloni, and J. M. Pastor, *Phys. Rev. E* **71**, 051303 (2005).
- [18] A. Janda, I. Zuriguel, A. Garcimartín, L. A. Pugnaloni, and D. Maza, *Europhys. Lett.* **84**, 44002 (2008).

- [19] S. Yang and S. Hsiau, *Powder Technol.* **120**, 244 (2001).
- [20] I. Zuriguel, A. Janda, A. Garcimartín, C. Lozano, R. Arévalo, and D. Maza, *Phys. Rev. Lett.* **107**, 278001 (2011).
- [21] F. Alonso-Marroquin, S. I. Azeezullah, S. A. Galindo-Torres, and L. M. Olsen-Kettle, *Phys. Rev. E* **85**, 020301(R) (2012).
- [22] C. Lozano, I. Zuriguel, A. Janda, A. Garcimartín, R. Arévalo, and D. Maza, in *Powders And Grains 2013: Proceedings of the 7th International Conference on Micromechanics of Granular Media*, edited by A. Yu, K. Dong, R. Yang, and S. Luding, AIP Conf. Proc. No. 1542 (American Institute of Physics, Melville, New York, 2013).
- [23] J. R. Johanson, *Powder Technol.* **1**, 328 (1968).
- [24] C. S. Chou and T. L. Yang, *Adv. Powder Technol.* **15**, 567 (2004).
- [25] C. S. Chou, C. Y. Tseng, and T. L. Yang, *J. Chin. Inst. Eng.* **29**, 1 (2006).
- [26] M. Wójcik, J. Tejchman, and G. G. Enstad, *Powder Technol.* **222**, 15 (2012).
- [27] J. Härtl, J. Y. Ooi, J. M. Rotter, M. Wąsjić, S. Ding, and G. G. Enstad, *Chem. Eng. Res. Des.* **86**, 370 (2008).
- [28] J. Horabik, P. Parafiniuk, and M. Molenda, *Powder Technol.* **327**, 320 (2018).
- [29] R. Kobylka, M. Molenda, and J. Horabik, *Powder Technol.* **343**, 521 (2019).
- [30] U. Tüzün and N. R. Nedderman, *Chem. Eng. Sci.* **40**, 325 (1985).
- [31] Q. Zhang, J. I. Bergen, and M. G. Britton, *Can. Agric. Eng.* **39**, 215 (1997).
- [32] S. Volpato, R. Artoni, and A. C. Santomaso, *Chem. Eng. Res. Des.* **92**, 256 (2014).
- [33] R. Kobylka and M. Molenda, *Powder Technol.* **256**, 210 (2014).
- [34] G. H. L. Hagen, *Ann. Phys. (Berlin, Ger.)* **46**, 423 (1839).
- [35] R. L. Brown and J. C. Richards, *Principles of Powder Mechanics* (Pergamon Press, Oxford, 1970).
- [36] R. L. Brown and J. C. Richards, *Trans. Inst. Chem. Eng.* **38**, 243 (1960).
- [37] R. M. Nedderman and C. Laohakul, *Powder Technol.* **25**, 91 (1980).
- [38] J. Y. Zhang and V. Rudolph, *Ind. Eng. Chem. Res.* **30**, 1977 (1991).
- [39] H. G. Sheldon and D. J. Durian, *Granular Matter* **12**, 579 (2010).
- [40] B. De-Song, Z. Xun-Sheng, X. Guang-Lei, P. Zheng-Quan, T. Xiao-Wei, and L. Kun-Quan, *Phys. Rev. E* **67**, 062301 (2003).
- [41] A. Guariguata, D. T. Wu, C. A. Koh, A. K. Sum, and E. D. Sloan, in *Proceedings of the 6th International Conference on Micromechanics of Granular Media*, edited by M. Nakagawa and S. Luding (American Institute of Physics, Melville, New York, 2009), pp. 543–546.
- [42] A. Guariguata, M. A. Pascall, M. W. Gilmer, A. K. Sum, E. D. Sloan, C. A. Koh, and D. T. Wu, *Phys. Rev. E* **86**, 061311 (2012).
- [43] P. G. Lafond, M. W. Gilmer, C. A. Koh, E. D. Sloan, D. T. Wu, and A. K. Sum, *Phys. Rev. E* **87**, 042204 (2013).
- [44] M. A. Aguirre, J. G. Grande, A. Calvo, L. A. Pugnaloni, and J.-C. Géminard, *Phys. Rev. Lett.* **104**, 238002 (2010).
- [45] M. A. Aguirre, J. G. Grande, A. Calvo, L. A. Pugnaloni, and J.-C. Géminard, *Phys. Rev. E* **83**, 061305 (2011).
- [46] M. J. Cordero and L. A. Pugnaloni, *Powder Technol.* **272**, 290 (2015).
- [47] C. Perge, M. A. Aguirre, P. A. Gago, L. A. Pugnaloni, D. Le Tourneau, and J.-C. Géminard, *Phys. Rev. E* **85**, 021303 (2012).
- [48] M. A. Aguirre, R. De Schant, and J.-C. Géminard, *Phys. Rev. E* **90**, 012203 (2014).
- [49] C. A. Schneider, W. S. Rasband, and K. W. Eliceiri, *Nat. Methods* **9**, 671 (2012).
- [50] D. Bideau, A. Gervois, L. Oger, and J. P. Troadec, *J. Phys. (Paris)* **47**, 1697 (1986).
- [51] Q. Zhang, B. Hao, and M. G. Britton, *Can. Biosyst. Eng.* **44**, 5.1 (2002).
- [52] C.-S. Chou, A.-F. Lee, and C.-K. Yeh, *Adv. Powder Technol.* **20**, 80 (2009).